Exploration of the origin of the excellent charge-carrier dynamics in Ruddlesden-Popper oxysulfide perovskite $Y_2Ti_2O_5S_2$

Yisen Yao[1,2], Qiaoqiao Li[3], Weibin Chu[5], Yi-min Ding[2], Luo Yan[3], Yang Gao[2,3], Arup Neogi[2], Alexander Govorov[2,4*], Liujiang Zhou[1,3*], Zhiming Wang[1,2*]

[1]*Institute of Fundamental and Frontier Sciences, University of Electronic Science and Technology of China, Chengdu 610054, China.*

[2]*Yangtze Delta Region Institute (Huzhou), University of Electronic Science and Technology of China, Huzhou 313001, China.*

[3] *School of Physics, University of Electronic Science and Technology of China, Chengdu 610054, China.*

[4] *Department of Physics and Astronomy, Ohio University, Athens, Ohio 45701, United States.*

[5] *Key Laboratory of Computational Physical Sciences (Ministry of Education), Institute of Computational Physical Sciences, Fudan University, Shanghai 200433, China.*

* Corresponding authors

Part 1 The orbital overlap features in $Y_2Ti_2O_5S_2$

The crystal orbital Hamilton populations (COHP) is calculated here to study the overlap between atoms (Figure 1S). The distance between two atoms can also reflect the bonding characteristics to a certain extent (Table 1). The distance between Y and S atoms is 2.82 Å, which is far from than Y−S single bond, indicating an ionic bond. The ELF Figure in text also confirmed this. However, there is still a little overlap between Y−d_{xy} and S−$p_{x,y}$ orbital that contributes to CBM and VBM, respectively (Figure 1S (b)). The distance between Ti and O atom is 1.82 Å, which is smaller than Ti−O single covalent bond, indicating a weak covalent bond between Ti and O atom. From Figure 1S (b) we can find no overlap between Ti−d_{xy} and S−$p_{x,y}$ orbital.

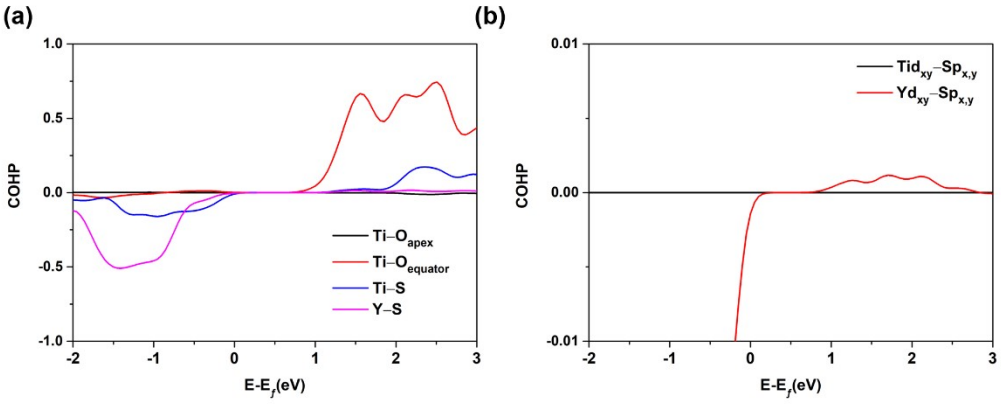

Figure S1. The COHP of selected atom (a) and selected orbital (b) in $Y_2Ti_2O_5S_2$. Ti–d_{xy} orbital and S–$p_{x,y}$ orbital are the major contributors to CBM and VBM individually. We can discover that the optical transition between Ti and S atoms cannot happen because of the no overlap between Ti–d_{xy} orbital and S–$p_{x,y}$ orbital.

Table S1. The table of bond length in our optimized structure and the covalent radii tested by Pekka Pyykkö.[1-4]

The bond length of $Y_2Ti_2O_5S_2$ (unit: Å)			
	$O_{equator}$	O_{apex}	S
Ti	1.82	1.96	2.92
Y	2.44	-	2.82
Covalent radii of the element involved in $Y_2Ti_2O_5S_2$ (Å)			
Ti single-bond		1.36	
Y single-bond		1.63	
O single-bond		0.63	
S single-bond		1.03	

Part 2 The transition dipole moment (TDM) of $Y_2Ti_2O_5S_2$，$CsPbI_3$ and Ta_3N_5.

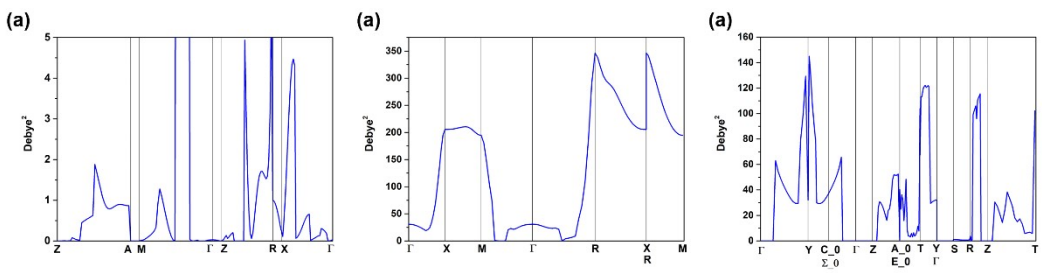

Figure S2. The TDM of $Y_2Ti_2O_5S_2$ (a), $CsPbI_3$ (b) and Ta_3N_5 (c). Although the transition at Γ point is allowed in $Y_2Ti_2O_5S_2$, it is still very weak compared to $CsPbI_3$ and Ta_3N_5.

Part 3 The influence spectra, uACF and pure-dephasing function

Hefei-named packages are used based on hopping probabilities between the two states obtained as[5]:

$$P_{j\to k}(t,\Delta t) = \frac{2R\left[c_j^* c_k d_{jk}\right]\Delta t}{c_j^* c_j} \qquad \text{E1}$$

$$d_{jk} = \left\langle \varphi_j \middle| \frac{\partial}{\partial t} \middle| \varphi_k \right\rangle = \sum_I \frac{\left\langle \varphi_j \middle| \nabla_{R_l} H \middle| \varphi_k \right\rangle}{\varepsilon_k - \varepsilon_j} \cdot \dot{R}_I \qquad \text{E2}$$

c are the coefficients of wave functions. d_{jk} is the NAC between Kohn–Sham states j and k. H is the Kohn-Sham Hamiltonian, φ_j, φ_k, ε_k and ε_j are the wave functions and eigenvalues for electron states j and k. $\dot{R}_I$ is velocity vector of the nuclei. $\left\langle \varphi_j \middle| \nabla_{R_l} H \middle| \varphi_k \right\rangle$ expresses the time-dependent orbital coupling including the overlap of two states. $\varepsilon_k - \varepsilon_j$ express the bandgap here. The elastic scattering can be presented by the decay time in pure-dephasing function and the unnormalized autocorrelation functions (uACF). The uACF can be written as:[6, 7]

$$C(t) = \langle \Delta E(t)\Delta E(0) \rangle_T \qquad \text{E3}$$

where $\Delta E(t) = E(t) - \langle E \rangle$ is the fluctuation of the energy gap between the two states forming a coherent superposition from its average value. The pure-dephasing function is given by:

$$D(t) = exp[-\frac{1}{\hbar^2}\int_0^t dt' \int_0^t dt'' C(t'')] \qquad \text{E4}$$

Fourier transforms (FTs) of the fluctuations for VBM-CBM energy gaps induced by phonon[6, 8, 9], named influence spectra or spectral density, can reflect the phonon mode that participates in e-ph coupling and is given by:

$$I(\omega) = \frac{1}{2\pi}\left| \int_{-\infty}^{+\infty} dt e^{-i\omega t} C(t) \right|^2 \qquad \text{E5}$$

Part 4 The distribution of band edge and ELF in $SrTiO_3$.

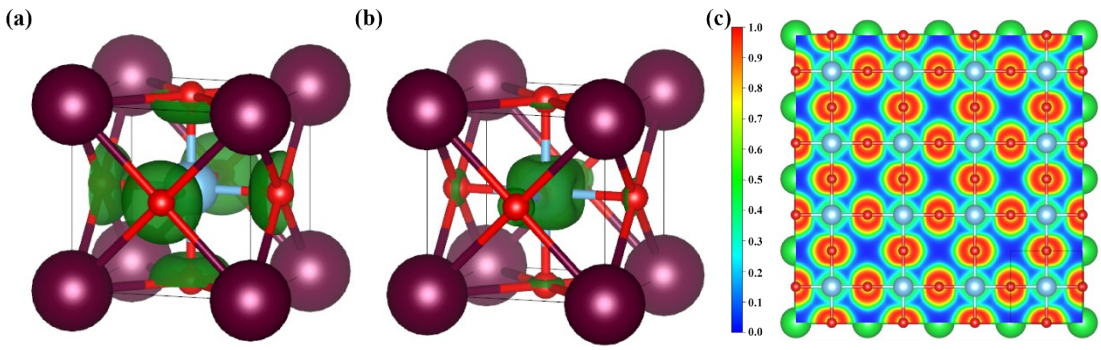

Figure S3 (a)(b) The partial charge density of VBM (a) and CBM (b) in $SrTiO_3$ with isosurface value 0.02 e/Å^3. (c) Electron localization function (ELF) in the (100) plane of $SrTiO_3$. The Ti–O bond is a mixture of ionic and covalent bonding, forming the network distribution of 0.2<ELF<0.7 in whole bulk.

Part 5 The weak exciton effect in $Y_2Ti_2O_5S_2$.

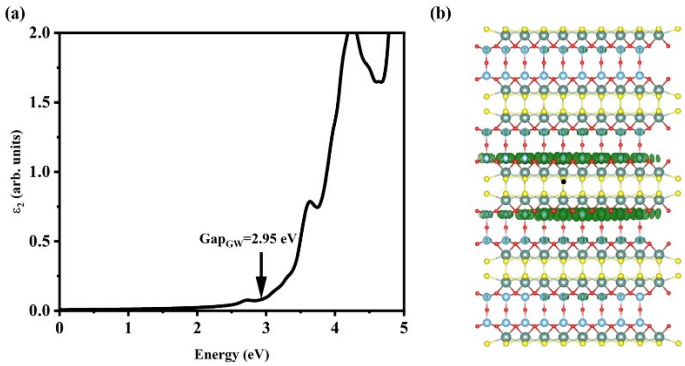

Figure S4 (a) The imaginary parts of the frequency-dependent dielectric function of $Y_2Ti_2O_5S_2$. The optical calculations with e-h interaction are presented, based on BSE level. (b) side view of exciton wave functions of $Y_2Ti_2O_5S_2$. A 5 × 5 × 1 supercell was adopted. The isovalue value is 8×10^{-9} e/Å^3. The hole position is marked by a black spot in the rock-salt layer. The electron mainly distributes in the perovskite layer, which finely explains its extremely small density distribution of excitons.

Part 6 The Robustness of electron-hole separated transport.

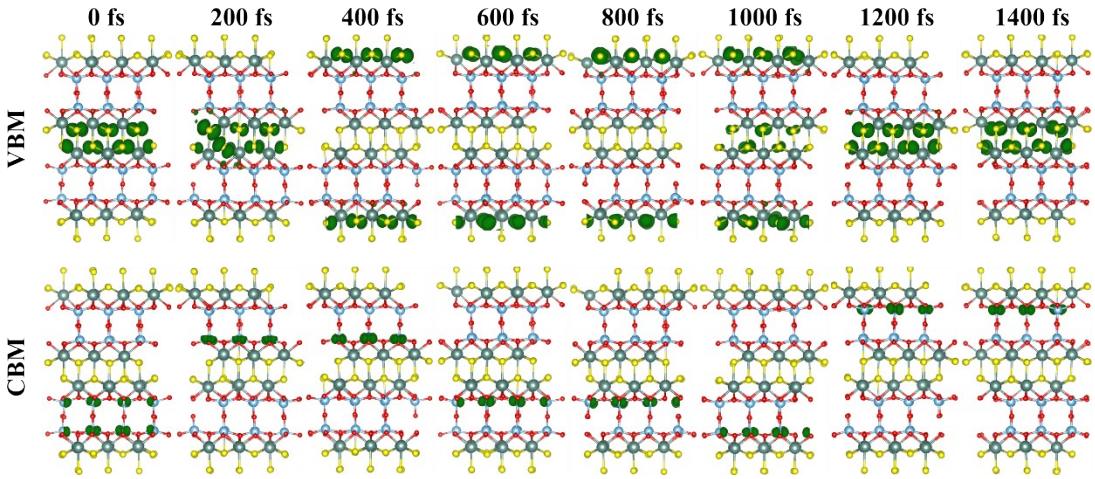

Figure S5 The VBM and CBM's partial charge density of snapshots at room temperature in $Y_2Ti_2O_5S_2$. We can find the robustness of electron-hole separated distribution, which is also the main character of electron-hole separated transport.

1. Pyykko, P.; Riedel, S.; Patzschke, M., Triple-bond covalent radii. *Chemistry-a European Journal* **2005,** *11* (12), 3511-3520.
2. Pyykko, P.; Atsumi, M., Molecular Double-Bond Covalent Radii for Elements Li-E112. *Chemistry-a European Journal* **2009,** *15* (46), 12770-12779.
3. Pyykko, P.; Atsumi, M., Molecular Single-Bond Covalent Radii for Elements 1-118. *Chemistry-a European Journal* **2009,** *15* (1), 186-197.
4. Pyykko, P., Refitted tetrahedral covalent radii for solids. *Phys. Rev. B* **2012,** *85* (2).
5. Zheng, Q. J.; Chu, W. B.; Zhao, C. Y.; Zhang, L. L.; Guo, H. L.; Wang, Y. N.; Jiang, X.; Zhao, J., Ab initio nonadiabatic molecular dynamics investigations on the excited carriers in condensed matter systems. *Wiley Interdiscip. Rev.-Comput. Mol. Sci.* **2019,** *9* (6), 27.
6. Li, W.; Liu, J.; Bai, F.-Q.; Zhang, H.-X.; Prezhdo, O. V., Hole Trapping by Iodine Interstitial Defects Decreases Free Carrier Losses in Perovskite Solar Cells: A Time-Domain Ab Initio Study. *ACS Energy Letters* **2017,** *2* (6), 1270-1278.
7. Zhang, Z.; Fang, W. H.; Tokina, M. V.; Long, R.; Prezhdo, O. V., Rapid Decoherence Suppresses Charge Recombination in Multi-Layer 2D Halide Perovskites: Time-Domain Ab Initio Analysis. *Nano Lett* **2018,** *18* (4), 2459-2466.
8. Li, W.; Tang, J.; Casanova, D.; Prezhdo, O. V., Time-Domain ab Initio Analysis Rationalizes the Unusual Temperature Dependence of Charge Carrier Relaxation in Lead Halide Perovskite. *ACS Energy Letters* **2018,** *3* (11), 2713-2720.
9. Long, R.; Fang, W.; Prezhdo, O. V., Moderate Humidity Delays Electron-Hole Recombination in Hybrid Organic-Inorganic Perovskites: Time-Domain Ab Initio Simulations Rationalize Experiments. *J Phys Chem Lett* **2016,** *7* (16), 3215-22.